Available online at www.sciencedirect.com
ScienceDirect
International Journal of Heat and Mass Transfer 50 (2007) 479–491
International Journal of HEAT and MASS TRANSFER
www.elsevier.com/locate/ijhmt

Velocity–vorticity formulation for 3D natural convection in an inclined cavity by DQ method

D.C. Lo [a], D.L. Young [b,*], K. Murugesan [c], C.C. Tsai [d], M.H. Gou [b]

[a] Institute of Marine Science and Technology, National Kaohsiung Marine University, Kaohsiung, 81157, Taiwan, ROC
[b] Department of Civil Engineering and Hydrotech Research Institute, National Taiwan University, Taipei 10617, Taiwan, ROC
[c] Department of Mechanical and Industrial Engineering, IIT Roorkee 247667, India
[d] Department of Information Technology, Toko University, Chia-Yi County 61363, Taiwan, ROC

Received 13 September 2005
Available online 11 October 2006

Abstract

The present work proposes a novel numerical solution algorithm based on a differential quadrature (DQ) method to simulate natural convection in an inclined cubic cavity using velocity–vorticity form of the Navier–Stokes equations. Since the DQ method employs a higher-order polynomial to approximate any given differential operator, the vorticity values at the boundaries can be computed more accurately than the conventionally followed second-order accurate Taylor's series expansion scheme. The numerical capability of the present algorithm is demonstrated by the application to natural convection in an inclined cubic cavity. The velocity Poisson equations, the continuity equation, the vorticity transport equations and the energy equation are all solved as a coupled system of equations for the seven field variables consisting of three velocities, three vorticities and temperature. Thus coupling the velocity and the vorticity transport equations allows the determination of the vorticity boundary values implicitly without requiring the explicit specification of the vorticity boundary conditions. The present algorithm is proved to be an efficient method to resolve the non-linearity involved with the vorticity transport equations and the energy equation. Test results obtained for an inclined cubic cavity with different angle of inclinations for Rayleigh number equal to 10^3, 10^4, 10^5 and 10^6 indicate that the present coupled solution algorithm could predict the benchmark results for temperature and flow fields using a much coarse computational grid compared to other numerical schemes.

Keywords: Velocity–vorticity formulation; Natural convection; Inclined cubic cavity; Differential quadrature method

1. Introduction

Numerical solution of incompressible Navier–Stokes equations is an important area in CFD related fields in science and engineering. With the development of a wide range of numerical schemes and algorithms, obtaining numerical solution of the Navier–Stokes equations now has become much easier compared to the previous decades. However, there is a continuous research going on in the development of new numerical algorithms as the CFD is used as a modeling tool in other areas of science as well. The velocity–vorticity formulation, pioneered by Fasel [1], is considered to be an alternate form of the Navier–Stokes equations without involving the pressure term. An important issue in the velocity–vorticity form of the Navier–Stokes equations is the enforcement of the vorticity definition on the boundary to assure divergence free velocity field. In many practical CFD problems, vortex dynamics has dominated the study of turbulence flow field for design purpose instead of the primitive variable form of the Navier–Stokes equations. Daube [2] pointed out that the satisfaction of the continuity equation reduces to enforce the vorticity definition at the boundaries in terms of curl of the velocity field. Moreover, the Navier–Stokes

* Corresponding author. Tel./fax: +886 2 2362 6114.
E-mail addresses: loderg@ntu.edu.tw (D.C. Lo), dlyoung@ntu.edu.tw (D.L. Young).

0017-9310/$ - see front matter © 2006 Elsevier Ltd. All rights reserved.
doi:10.1016/j.ijheatmasstransfer.2006.07.025

equations in velocity–vorticity form indicate that vorticity is created at the boundary in such a way that it satisfies the velocity boundary conditions [3]. By definition, the vorticity is defined as the curl of the velocity field and hence in order to exactly satisfy the vorticity definition at the boundary, accurate computation of velocity gradients are very crucial. Especially when fully discretized form of the velocity–vorticity equations are solved using numerical schemes based on grid or cell discretization, a suitable computational procedure has to be followed to compute the vorticity values at the boundary so that the vorticity definition is completely satisfied at the boundary nodes. Further, in order to enforce the solenoidality of vorticity in a three-dimensional flow field, the solution of the vorticity transport equations depends on the accurate computation of the vorticity values at the boundaries [3–5].

Generally the vorticity boundary values are determined explicitly using a second-order accurate Taylor's series expansion scheme [6] while computing flow fields using the velocity–vorticity form of the Navier–Stokes equations. Hence care must be taken to assure accurate computation of the vorticity values at the boundaries by using finer mesh near the boundaries when lower-order schemes are used for vorticity definition. The use of the differential quadrature method enables the computation of vorticity definition with higher-order polynomials. Because any given derivative with respect to a coordinate direction is approximated using a polynomial order closer to the number of grid points considered in that particular coordinate direction. Furthermore, when a coupled numerical scheme involving a global method of differential quadrature (DQ) method is used to solve the governing equations, the explicit specification of vorticity definition at the boundary is completely eliminated, resulting in a simplified computational procedure.

It should be noted that the curl of the momentum equations in primitive variable form gives rise to the dynamic vorticity transport equations. Also, the curl of vorticity definition, results in the kinematic velocity Poisson equations for the velocity field. Guj and Stella [3] pointed out the solenoidal velocity field can be assured only by coupling the kinematic and the dynamic equations. In the present work, the velocities u and v in the x-direction and y-direction are obtained by solving the Poisson equations; the velocity w in the z-direction is determined from the continuity equation, thus assuring a divergence-free velocity field [7]. On the other hand, the vorticity and the temperature fields can be obtained by solving the vorticity transport equations and the energy equation, respectively. When higher-order approximation is used to compute all the flow field variables, a numerical coupling between the velocity, vorticity and temperature are required to satisfy the conservative form of the velocity and the vorticity fields. The motivation for the present work originated from the fact that how to enforce the vorticity definition accurately as the curl of velocity. By coupling the entire field variables the vorticity boundary values can be computed implicitly from the vorticity definition without needing explicit specification of the known vorticity values.

The DQ method was first pioneered by Bellman et al. [8] to approximate the derivative of a smooth function and has been successfully implemented for solving many engineering problems [4,9–12]. Shu and Xue [10] applied the generalized differential quadrature method to simulate natural convection in a square cavity. Two boundary conditions (Dirichlet and Neumann type) for the stream function at each boundary were addressed in detail therein. The present study proposes a novel idea to solve three-dimensional Navier–Stokes equations by efficiently exploiting the advantages of both the velocity–vorticity form of the Navier–Stokes equations and the DQ method. Natural convection in a differentially heated inclined cubic cavity is represented by continuity equation, momentum equations and energy equation, which are coupled due to the buoyancy term appearing in the momentum equation. Hence natural convection in an inclined cubic cavity is considered to be the best example problem to test the numerical capability of the proposed coupled algorithm. All the seven field variables involving three velocities, three vorticities and temperature are solved using a single global matrix as a coupled system of variables.

The proposed numerical scheme is applied to determine the velocity, vorticity and temperature variations for natural convection problem in a differentially heated inclined cubic cavity for Rayleigh number range from 10^3 to 10^6. Numerical formulation, solution procedure and comparisons of the present results with those obtained by other numerical schemes are presented in the following sections.

2. Differential quadrature method

The DQ method replaces a given spatial derivative of a function $f(x)$ by a linear weighted sum of the function values at the discrete sample points considered along a coordinate direction, resulting in a set of algebraic equations. Hence the DQ method can be used to obtain numerical solution of partial differential equations with higher-order accuracy. The details about this method can be obtained in Refs. [9,12]. For a function of three variables $f(x,y,z)$, the pth-order derivatives, qth-order derivatives and rth-order derivatives of the function with respect to x, y and z coordinates can be obtained as

$$f_x^{(p)}(x_i,y_j,z_k)=\sum_{l=1}^{L}A_{i,l}^{(p)}f(x_l,y_j,z_k),\quad p=1,2,\ldots,L-1 \tag{1a}$$

$$f_y^{(q)}(x_i,y_j,z_k)=\sum_{m=1}^{M}B_{j,m}^{(q)}f(x_i,y_m,z_k),\quad q=1,2,\ldots,M-1 \tag{1b}$$

$$f_z^{(r)}(x_i,y_j,z_k)=\sum_{n=1}^{N}C_{k,n}^{(r)}f(x_i,y_j,z_n),\quad r=1,2,\ldots,N-1 \tag{1c}$$

$$\text{for } i=1,2,\ldots,L;\ j=1,2,\ldots,M;\ k=1,2,\ldots,N$$

where l, m, n are the indices for the grid points in the x-, y- and z-coordinates respectively, L, M, N are the number of grid points in the x-, y-, z-directions, respectively and $A^{(p)}_{i,l}, B^{(q)}_{j,m}, C^{(r)}_{k,n}$ are the weighting coefficients. The first-order weighting coefficients $A^{(1)}_{i,l}, B^{(1)}_{j,m}, C^{(1)}_{k,n}$ can be determined as follows:

$$A^{(1)}_{i,j} = \frac{L^{(1)}(x_i)}{(x_i - x_j)L^{(1)}(x_j)}, \quad i,j = 1,2,\ldots,L, \quad \text{but } j \neq i \tag{2a}$$

$$B^{(1)}_{i,j} = \frac{M^{(1)}(y_i)}{(y_i - y_j)M^{(1)}(y_j)}, \quad i,j = 1,2,\ldots,M, \quad \text{but } j \neq i \tag{2b}$$

$$C^{(1)}_{i,j} = \frac{N^{(1)}(z_i)}{(z_i - z_j)N^{(1)}(z_j)}, \quad i,j = 1,2,\ldots,N, \quad \text{but } j \neq i \tag{2c}$$

in which

$$L^{(1)}(x_i) = \prod_{j=1, j\neq i}^{L} (x_i - x_j),$$

$$M^{(1)}(y_i) = \prod_{j=1, j\neq i}^{M} (y_i - y_j), \quad N^{(1)}(z_i) = \prod_{j=1, j\neq i}^{N} (z_i - z_j) \tag{3}$$

Similarly the weighting coefficients for the second- and higher-order derivatives can be obtained as

$$A^{(p)}_{i,j} = p\left(A^{(p-1)}_{i,i} A^{(1)}_{i,j} - \frac{A^{(p-1)}_{i,j}}{x_i - x_j}\right), \quad \text{for } i,j = 1,2,\ldots,L,$$
$$\text{but } j \neq i, \ l = 2,3,\ldots,L-1 \tag{4a}$$

$$B^{(q)}_{i,j} = q\left(B^{(q-1)}_{i,i} B^{(1)}_{i,j} - \frac{B^{(q-1)}_{i,j}}{y_i - y_j}\right), \quad \text{for } i,j = 1,2,\ldots,M,$$
$$\text{but } j \neq i, \ m = 2,3,\ldots,M-1 \tag{4b}$$

$$C^{(r)}_{i,j} = r\left(C^{(r-1)}_{i,i} C^{(1)}_{i,j} - \frac{C^{(r-1)}_{i,j}}{z_i - z_j}\right), \quad \text{for } i,j = 1,2,\ldots,N,$$
$$\text{but } j \neq i, \ n = 2,3,\ldots,N-1 \tag{4c}$$

When $j = i$, the weighting coefficients are written as

$$A^{(p)}_{i,i} = -\sum_{j=1, j\neq i}^{L} A^{(p)}_{i,j}, \quad i = 1,2,\ldots,L, \ p = 1,2,\ldots,L-1 \tag{5a}$$

$$B^{(q)}_{i,i} = -\sum_{j=1, j\neq i}^{M} B^{(q)}_{i,j}, \quad i = 1,2,\ldots,M, \ q = 1,2,\ldots,M-1 \tag{5b}$$

$$C^{(r)}_{i,i} = -\sum_{j=1, j\neq i}^{N} C^{(r)}_{i,j}, \quad i = 1,2,\ldots,N, \ r = 1,2,\ldots,N-1 \tag{5c}$$

It should be noted from the above equations that the weighting coefficients of the second- and higher-order derivatives can be computed from the first-order derivatives themselves.

3. Governing equations

The governing equations for natural convection can be described by the incompressible Navier–Stokes equations and the energy equation. Assuming the Boussinesq approximation, the velocity–vorticity form of the Navier–Stokes equations can be written in a non-dimensional form as follows:

Velocity Poisson equations

$$\nabla^2 u = -\frac{\partial \zeta}{\partial y} + \frac{\partial \eta}{\partial z} \tag{6a}$$

$$\nabla^2 v = -\frac{\partial \xi}{\partial z} + \frac{\partial \zeta}{\partial x} \tag{6b}$$

$$\nabla^2 w = -\frac{\partial \eta}{\partial x} + \frac{\partial \xi}{\partial y} \tag{6c}$$

Vorticity transport equations

$$\frac{\partial \xi}{\partial t} + u\frac{\partial \xi}{\partial x} + v\frac{\partial \xi}{\partial y} + w\frac{\partial \xi}{\partial z} = \xi\frac{\partial u}{\partial x} + \eta\frac{\partial u}{\partial y} + \zeta\frac{\partial u}{\partial z} + Pr(\nabla^2 \xi) + RaPr\cos\phi\left(\frac{\partial T}{\partial y}\right) \tag{7a}$$

$$\frac{\partial \eta}{\partial t} + u\frac{\partial \eta}{\partial x} + v\frac{\partial \eta}{\partial y} + w\frac{\partial \eta}{\partial z} = \xi\frac{\partial v}{\partial x} + \eta\frac{\partial v}{\partial y} + \zeta\frac{\partial v}{\partial z} + Pr(\nabla^2 \eta) + RaPr\left(\sin\phi\frac{\partial T}{\partial z} - \cos\phi\frac{\partial T}{\partial x}\right) \tag{7b}$$

$$\frac{\partial \zeta}{\partial t} + u\frac{\partial \zeta}{\partial x} + v\frac{\partial \zeta}{\partial y} + w\frac{\partial \zeta}{\partial z} = \xi\frac{\partial w}{\partial x} + \eta\frac{\partial w}{\partial y} + \zeta\frac{\partial w}{\partial z} + Pr(\nabla^2 \zeta) - RaPr\sin\phi\left(\frac{\partial T}{\partial y}\right) \tag{7c}$$

Energy equation

$$\frac{\partial T}{\partial t} + u\frac{\partial T}{\partial x} + v\frac{\partial T}{\partial y} + w\frac{\partial T}{\partial z} = \nabla^2 T \tag{8}$$

The main focus of the present numerical solution procedure is to compute divergence-free velocity field for coupled problems using coarse mesh compared to other numerical schemes. After computing the u and the v velocity components, the w velocity component can be obtained either using Eq. (6c) or the divergence of the continuity equation with respect to the z-direction as given below:

$$\frac{\partial^2 u}{\partial x \partial z} + \frac{\partial^2 v}{\partial y \partial z} + \frac{\partial^2 w}{\partial z^2} = 0 \tag{9}$$

It should be noted that the velocity Poisson equations (6a)–(6c) have been obtained only after satisfying the continuity constraint. Hence computing the w velocity using Eq. (9) becomes an indirect verification for the correct determination of the u and the v velocity components and also it reduces the computational time as discussed by Wu et al. [7].

The computational domain is discretized using a Cartesian coordinate frame with x–y representing the horizontal plane and z directing in the vertical direction. In the velocity–vorticity form of the Navier–Stokes equations, the vorticity vector is defined as

$$\vec{\omega} = \nabla \times \vec{u} \tag{10}$$

where $\vec{u} = (u, v, w)$ and $\vec{\omega} = (\xi, \eta, \varsigma)$ are the velocity and the vorticity vectors in the x-, y- and z-directions, respectively.

The non-dimensional parameters are defined as, Prandtl number, $Pr = \frac{\upsilon}{\alpha}$ and Rayleigh number, $Ra = \frac{g\beta\Delta TL^3}{\alpha\upsilon}$.

Eqs. (6a), (6b), (7a)–(7c), (8), (9) are the final form of the governing equations that characterize the flow and heat transfer during a natural convection process. These equations have to be solved in a computational domain Ω which is enclosed by a solid boundary Γ. For the problem of natural convection in a differentially heated cubic cavity, no-slip velocity boundary conditions are assumed on all the boundary walls. The Dirichlet boundary conditions for velocity on all the walls can be imposed as

$$\vec{u} = \vec{u}_b = 0 \tag{11}$$

The boundary conditions for the vorticity transport equations are computed from its definition given by Eq. (10). The energy equation is solved by assuming Dirichlet temperature boundary conditions equal to -0.5 and 0.5, respectively on the left and the right walls of the cavity and the other walls of the cavity are assumed to be adiabatic for heat transport. The Dirichlet and the Neumann boundary conditions for the energy equation can be written respectively as

$$T = T_b \tag{12a}$$

$$\frac{\partial T}{\partial y} = 0, \quad \frac{\partial T}{\partial z} = 0 \tag{12b}$$

4. Numerical solution

In order to achieve a significant saving in the computational effort, a coupled solution scheme via a single global matrix is adopted to compute all the field variables. Using this coupled algorithm, the boundary vorticity values are computed implicitly, without the need to compute the boundary vorticity values externally using a separate scheme such as the Taylor's series expansion scheme adopted by Wong and Baker [6]. The coupled algorithm has also enabled the implicit enforcement of the kinematic Poisson equations as well as the coupling of the velocity and the vorticity at the wall. In addition to this, the use of the DQ method enables the approximation of the vorticity definition at the boundaries with higher-order accuracy using only a coarse mesh. Hence the continuity constraint and the conservation of the solenoidality of vorticity field are easily satisfied in the proposed coupled algorithm. The time derivatives of the vorticity transport equations and the energy equation are discretized using a semi-implicit Adams-Bashforth/backward-differentiation scheme expressed as

$$\begin{aligned}&\frac{\partial G}{\partial t} + u\cdot\nabla G + \nabla^2 G = f\\ &\Rightarrow \frac{3G^{t+1} - 4G^t + G^{t-1}}{2\Delta t} + 2u^t\cdot\nabla G^t - u^{t-1}\cdot\nabla G^{t-1} + \nabla^2 G^{t+1}\\ &= f^{t+1}\end{aligned} \tag{13}$$

4.1. Approximation of the governing equations using the DQ method

Application of the DQ method to spatial discretization of the governing equations results in a set of algebraic equations. The velocity Poisson equations (6a) and (6b) and the continuity equation (9) are approximated using the DQ method to obtain the velocity components in the three coordinate directions, respectively, as

$$\sum_{l=1}^{L} A_{i,l}^{(2)} u_{l,j,k} + \sum_{m=1}^{M} B_{j,m}^{(2)} u_{i,m,k} + \sum_{n=1}^{N} C_{k,n}^{(2)} u_{i,j,n} + \sum_{m=1}^{M} B_{j,m}^{(1)} \zeta_{i,m,k} - \sum_{n=1}^{N} C_{k,n}^{(1)} \eta_{i,j,n} = 0 \tag{14a}$$

$$\sum_{l=1}^{L} A_{i,l}^{(2)} v_{l,j,k} + \sum_{m=1}^{M} B_{j,m}^{(2)} v_{i,m,k} + \sum_{n=1}^{N} C_{k,n}^{(2)} v_{i,j,n} - \sum_{l=1}^{L} A_{i,l}^{(1)} \zeta_{l,j,k} + \sum_{n=1}^{N} C_{k,n}^{(1)} \xi_{i,j,n} = 0 \tag{14b}$$

$$\sum_{l=1}^{L} A_{i,l}^{(1)} \sum_{n=1}^{N} C_{k,n}^{(1)} u_{l,j,n} + \sum_{m=1}^{M} B_{j,m}^{(1)} \sum_{n=1}^{N} C_{k,n}^{(1)} v_{i,m,n} + \sum_{n=1}^{N} C_{k,n}^{(2)} w_{i,j,n} = 0 \tag{14c}$$

The vorticity transport equations (7a)–(7c) are approximated for the solution of the vorticity components in the three coordinate directions as follows:

$$\begin{aligned}&\frac{(3\xi_{i,j,k})^{t+1}}{2\Delta t} - Pr\left(\sum_{l=1}^{L} A_{i,l}^{(2)} \xi_{l,j,k} + \sum_{m=1}^{M} B_{j,m}^{(2)} \xi_{i,m,k} + \sum_{n=1}^{N} C_{k,n}^{(2)} \xi_{i,j,n}\right)^{t+1}\\ &\quad - RaPr\cos\phi\left(\sum_{m=1}^{M} B_{j,m}^{(1)} T_{i,m,k}\right)^{t+1}\\ &= \frac{(4\xi_{i,j,k})^{t}}{2\Delta t} - \frac{(\xi_{i,j,k})^{t-1}}{2\Delta t}\\ &\quad - 2\left(u_{i,j,k}\sum_{l=1}^{L} A_{i,l}^{(1)} \xi_{l,j,k} + v_{i,j,k}\sum_{m=1}^{M} B_{j,m}^{(1)} \xi_{i,m,k} + w_{i,j,k}\sum_{n=1}^{N} C_{k,n}^{(1)} \xi_{i,j,n}\right)^{t}\\ &\quad + \left(u_{i,j,k}\sum_{l=1}^{L} A_{i,l}^{(1)} \xi_{l,j,k} + v_{i,j,k}\sum_{m=1}^{M} B_{j,m}^{(1)} \xi_{i,m,k} + w_{i,j,k}\sum_{n=1}^{N} C_{k,n}^{(1)} \xi_{i,j,n}\right)^{t-1}\\ &\quad + 2\left(\xi_{i,j,k}\sum_{l=1}^{L} A_{i,l}^{(1)} u_{l,j,k} + \eta_{i,j,k}\sum_{m=1}^{M} B_{j,m}^{(1)} u_{i,m,k} + \zeta_{i,j,k}\sum_{n=1}^{N} C_{k,n}^{(1)} u_{i,j,n}\right)^{t}\\ &\quad - \left(\xi_{i,j,k}\sum_{l=1}^{L} A_{i,l}^{(1)} u_{l,j,k} + \eta_{i,j,k}\sum_{m=1}^{M} B_{j,m}^{(1)} u_{i,m,k} + \zeta_{i,j,k}\sum_{n=1}^{N} C_{k,n}^{(1)} u_{i,j,n}\right)^{t-1}\end{aligned} \tag{15a}$$

$$\frac{(3\eta_{i,j,k})^{t+1}}{2\Delta t} - Pr\left(\sum_{l=1}^{L} A_{i,l}^{(2)}\eta_{l,j,k} + \sum_{m=1}^{M} B_{j,m}^{(2)}\eta_{i,m,k} + \sum_{n=1}^{N} C_{k,n}^{(2)}\eta_{i,j,n}\right)^{t+1} - RaPr\left(\sin\phi\sum_{n=1}^{N} C_{k,n}^{(1)}T_{i,j,n} - \cos\phi\sum_{l=1}^{L} A_{i,l}^{(1)}T_{l,j,k}\right)^{t+1} = \frac{(4\eta_{i,j,k})^{t}}{2\Delta t} - \frac{(\eta_{i,j,k})^{t-1}}{2\Delta t} - 2\left(u_{i,j,k}\sum_{l=1}^{L} A_{i,l}^{(1)}\eta_{l,j,k} + v_{i,j,k}\sum_{m=1}^{M} B_{j,m}^{(1)}\eta_{i,m,k} + w_{i,j,k}\sum_{n=1}^{N} C_{k,n}^{(1)}\eta_{i,j,n}\right)^{t} + \left(u_{i,j,k}\sum_{l=1}^{L} A_{i,l}^{(1)}\eta_{l,j,k} + v_{i,j,k}\sum_{m=1}^{M} B_{j,m}^{(1)}\eta_{i,m,k} + w_{i,j,k}\sum_{n=1}^{N} C_{k,n}^{(1)}\eta_{i,j,n}\right)^{t-1} + 2\left(\xi_{i,j,k}\sum_{l=1}^{L} A_{i,l}^{(1)}v_{l,j,k} + \eta_{i,j,k}\sum_{m=1}^{M} B_{j,m}^{(1)}v_{i,m,k} + \zeta_{i,j,k}\sum_{n=1}^{N} C_{k,n}^{(1)}v_{i,j,n}\right)^{t} - \left(\xi_{i,j,k}\sum_{l=1}^{L} A_{i,l}^{(1)}v_{l,j,k} + \eta_{i,j,k}\sum_{m=1}^{M} B_{j,m}^{(1)}v_{i,m,k} + \zeta_{i,j,k}\sum_{n=1}^{N} C_{k,n}^{(1)}v_{i,j,n}\right)^{t-1} \tag{15b}$$

$$\frac{(3\zeta_{i,j,k})^{t+1}}{2\Delta t} - Pr\left(\sum_{l=1}^{L} A_{i,l}^{(2)}\zeta_{l,j,k} + \sum_{m=1}^{M} B_{j,m}^{(2)}\zeta_{i,m,k} + \sum_{n=1}^{N} C_{k,n}^{(2)}\zeta_{i,j,n}\right)^{t+1} + RaPr\cos\phi\left(\sum_{m=1}^{M} B_{j,m}^{(1)}T_{i,m,k}\right)^{t+1} = \frac{(4\zeta_{i,j,k})^{t}}{2\Delta t} - \frac{(\zeta_{i,j,k})^{t-1}}{2\Delta t} - 2\left(u_{i,j,k}\sum_{l=1}^{L} A_{i,l}^{(1)}\zeta_{l,j,k} + v_{i,j,k}\sum_{m=1}^{M} B_{j,m}^{(1)}\zeta_{i,m,k} + w_{i,j,k}\sum_{n=1}^{N} C_{k,n}^{(1)}\zeta_{i,j,n}\right)^{t} + \left(u_{i,j,k}\sum_{l=1}^{L} A_{i,l}^{(1)}\zeta_{l,j,k} + v_{i,j,k}\sum_{m=1}^{M} B_{j,m}^{(1)}\zeta_{i,m,k} + w_{i,j,k}\sum_{n=1}^{N} C_{k,n}^{(1)}\zeta_{i,j,n}\right)^{t-1} + 2\left(\xi_{i,j,k}\sum_{l=1}^{L} A_{i,l}^{(1)}w_{l,j,k} + \eta_{i,j,k}\sum_{m=1}^{M} B_{j,m}^{(1)}w_{i,m,k} + \zeta_{i,j,k}\sum_{n=1}^{N} C_{k,n}^{(1)}w_{i,j,n}\right)^{t} - \left(\xi_{i,j,k}\sum_{l=1}^{L} A_{i,l}^{(1)}w_{l,j,k} + \eta_{i,j,k}\sum_{m=1}^{M} B_{j,m}^{(1)}w_{i,m,k} + \zeta_{i,j,k}\sum_{n=1}^{N} C_{k,n}^{(1)}w_{i,j,n}\right)^{t-1} \tag{15c}$$

Finally the DQ form of the energy equation is written as

$$\frac{(3T_{i,j,k})^{t+1}}{2\Delta t} - \left(\sum_{l=1}^{L} A_{i,l}^{(2)}T_{l,j,k} + \sum_{m=1}^{M} B_{j,m}^{(2)}T_{i,m,k} + \sum_{n=1}^{N} C_{k,n}^{(2)}T_{i,j,n}\right)^{t+1} = \frac{(4T_{i,j,k})^{t}}{2\Delta t} - \frac{(T_{i,j,k})^{t-1}}{2\Delta t} - 2\left(u_{i,j,k}\sum_{l=1}^{L} A_{i,l}^{(1)}T_{l,j,k} + v_{i,j,k}\sum_{m=1}^{M} B_{j,m}^{(1)}T_{i,m,k} + w_{i,j,k}\sum_{n=1}^{N} C_{k,n}^{(1)}T_{i,j,n}\right)^{t} + \left(u_{i,j,k}\sum_{l=1}^{L} A_{i,l}^{(1)}T_{l,j,k} + v_{i,j,k}\sum_{m=1}^{M} B_{j,m}^{(1)}T_{i,m,k} + w_{i,j,k}\sum_{n=1}^{N} C_{k,n}^{(1)}T_{i,j,n}\right)^{t-1} \tag{16}$$

4.2. Determination of vorticity boundary conditions

The vorticity boundary conditions for all the three vorticity transport equations in the principal coordinate directions are computed using the vorticity definition given by Eq. (10). The velocity gradients used in this definition are computed using a polynomial expression with the highest-order polynomial equal to $(N-1)$ where N is the number of grid points in the given coordinate direction, as expressed by the first-order weighting coefficients $A_{i,l}^{(1)}, B_{j,m}^{(1)}, C_{k,n}^{(1)}$. By applying the DQ approximation to the vorticity definition given by Eq. (10) the three vorticity components on a boundary can be expressed as

$$\xi_{i,j,k} - \sum_{m=1}^{M} B_{j,m}^{(1)}w_{i,m,k} + \sum_{n=1}^{N} C_{k,n}^{(1)}v_{i,j,n} = 0 \tag{17a}$$

$$\eta_{i,j,k} + \sum_{l=1}^{L} A_{i,l}^{(1)}w_{l,j,k} - \sum_{n=1}^{N} C_{k,n}^{(1)}u_{i,j,n} = 0 \tag{17b}$$

$$\zeta_{i,j,k} - \sum_{l=1}^{L} A_{i,l}^{(1)}v_{l,j,k} + \sum_{m=1}^{M} B_{j,m}^{(1)}u_{i,m,k} = 0 \tag{17c}$$

The Dirichlet boundary conditions for the temperature are expressed as

$$\begin{aligned} T_{L,j,k} &= 0.5, \quad j = 1,\ldots,M,\ k = 1,\ldots,N \\ T_{1,j,k} &= -0.5, \quad j = 1,\ldots,M,\ k = 1,\ldots,N \end{aligned} \tag{18}$$

The adiabatic boundary conditions are enforced by computing the normal derivatives of the temperature at the adiabatic walls and equating them to zero. Hence the DQ form of the adiabatic boundary conditions can be represented in the following expressions:

$$\sum_{m=1}^{M} B_{j,m}^{(1)}T_{i,m,k} = 0, \quad i = 2,\ldots,L-1,\ k = 1,\ldots,N,\ j = 1,M \tag{19a}$$

$$\sum_{n=1}^{N} C_{k,n}^{(1)}T_{i,j,n} = 0, \quad i = 2,\ldots,L-1,\ j = 1,\ldots,M,\ k = 1,L \tag{19b}$$

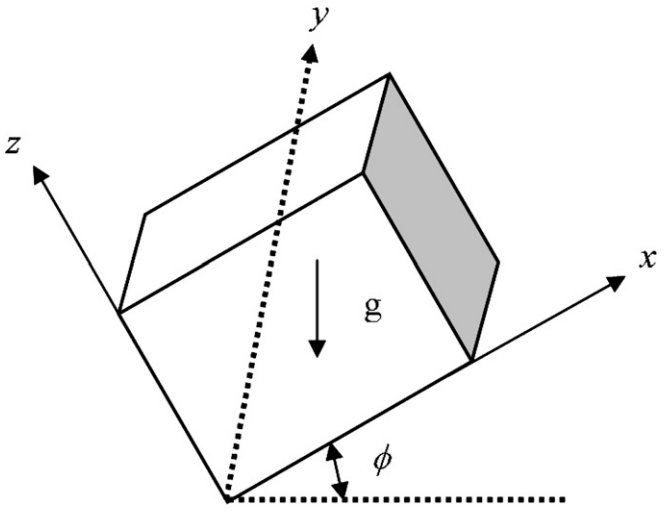

Fig. 1. Layout of the problem.

Eqs. (19a) and (19b) also involve the implicit scheme for the Neumann boundary conditions.

4.3. Solution procedure

The simultaneous equations resulting from the single global matrix system of equation are solved using a BICG iterative solver [13]. Since the coefficient matrix of the global matrix system is sparse, only the non-zero entries are stored in a column storage format. In the successive time step, we used the velocity, vorticity and temperature components at the previous time step as the initial guesses for the next iteration. The computations are carried out until steady state conditions are reached.

The convergence criteria used in the time loop to achieve steady state conditions are

$$\begin{aligned} &|(u^{t+1}-u^t)/u^t| \leqslant 10^{-6}, \quad |(v^{t+1}-v^t)/v^t| \leqslant 10^{-6}, \\ &|(w^{t+1}-w^t)/w^t| \leqslant 10^{-6}, \quad |(\xi^{t+1}-\xi^t)/\xi^t| \leqslant 10^{-6}, \\ &|(\eta^{t+1}-\eta^t)/\eta^t| \leqslant 10^{-6}, \quad |(\zeta^{t+1}-\zeta^t)/\zeta^t| \leqslant 10^{-6}, \\ &|(T^{t+1}-T^t)/T^t| \leqslant 10^{-6} \end{aligned} \tag{20}$$

For the DQ method, the mesh point distribution in the three spatial coordinates is assumed to be the same and is expressed as

Table 1
Grid-independence study results for $Ra = 10^3, 10^4, 10^5, 10^6$

Ra	Nusselt number	PSC (81^3) [14]	DQ method			
			21^3 grids	23^3 grids	25^3 grids	41^3 grids
$Ra = 10^3$	Nu_{mean}	1.0873	1.0870	1.0870	1.0870	1.0870
	Error (%)		0.0276	0.0276	0.0276	0.0276
	Nu_{over}	1.0700	1.0700	1.0700	1.0700	1.0700
	Error (%)		0.0000	0.0000	0.0000	0.0000
$Ra = 10^4$	Nu_{mean}	2.2505	2.2534	2.2510	2.2510	2.2510
	Error (%)		0.1289	0.0222	0.0222	0.0222
	Nu_{over}	2.0542	2.0522	2.0545	2.0540	2.0540
	Error (%)		0.0974	0.0146	0.0097	0.0097
$Ra = 10^5$	Nu_{mean}	4.6127	4.6241	4.6176	4.6100	4.6100
	Error (%)		0.2471	0.1062	0.0585	0.0585
	Nu_{over}	4.3371	4.3292	4.3341	4.3350	4.3350
	Error (%)		0.1821	0.0692	0.0484	0.0484
$Ra = 10^6$	Nu_{mean}	8.8771	8.9099	8.9098	8.9098	8.9098
	Error (%)		0.3690	0.3684	0.3678	0.3678
	Nu_{over}	8.6407	8.6694	8.6691	8.6678	8.6678
	Error (%)		0.3321	0.3287	0.3136	0.3136

Table 2
Numerical results for $Ra = 10^3$ at different angles

Ra		0°		15°		30°		45°		60°	
Nu_{mean}		1.0884		1.0731		1.0533		1.0329		1.0156	
Nu_{over}		1.0710		1.0590		1.0432		1.0268		1.0127	
10^3											
u_{max}	x		0.0000		0.0000		0.0000		0.0000		0.0000
	y	3.5227	0.5000	3.1766	0.5000	2.6870	0.5000	2.0940	0.5000	1.4310	0.5000
	z		0.1956		0.1956		0.1956		0.1956		0.1956
v_{max}	x		0.0000		0.0000		0.0000		0.0000		0.2500
	y	0.1726	0.2500	0.1385	0.2500	0.0982	0.2500	0.0593	0.2500	0.0330	0.8044
	z		0.5000		0.5000		0.5000		0.5000		0.1033
w_{max}	x		0.3044		0.3044		0.3044		0.3044		0.3044
	y	3.5163	0.5000	3.1850	0.5000	2.7063	0.5000	2.1176	0.5000	1.4519	0.5000
	z		0.5000		0.5000		0.5000		0.5000		0.5000
u_{mmax}	x	3.5227	0.0000	3.1766	0.0000	2.6870	0.0000	2.6870	0.0000	1.4310	0.000
	z		0.1956		0.1956		0.1956		0.1956		0.196
w_{mmax}	x	3.5163	0.3044	3.1850	0.3044	2.7063	0.3044	2.7063	0.3044	1.4519	0.304
	z		0.5000		0.5000		0.5000		0.5000		0.500

$$x_i = \frac{\cos[\pi/(2L)] - \cos[(2i-1)\pi/(2L)]}{\cos[\pi/(2L)] - \cos[(2L-1)\pi/(2L)]}, \quad i = 1,2,\ldots,L$$
$$y_j = \frac{\cos[\pi/(2M)] - \cos[(2j-1)\pi/(2M)]}{\cos[\pi/(2M)] - \cos[(2M-1)\pi/(2M)]}, \quad j = 1,2,\ldots,M$$
$$z_k = \frac{\cos[\pi/(2N)] - \cos[(2k-1)\pi/(2N)]}{\cos[\pi/(2N)] - \cos[(2N-1)\pi/(2N)]}, \quad k = 1,2,\ldots,N \tag{21}$$

where L, M, N are the number of grid points in the x-, y- and z-directions, respectively.

5. Numerical results

The schematic diagram of the inclined cubic cavity with the boundary conditions for the natural convection problem is displayed in Fig. 1. Temperatures equal to -0.5 and 0.5 are enforced on the left wall at $x = -0.5$ and the right wall at $x = 0.5$, respectively. Numerical results obtained for the test problem are discussed in this section.

5.1. Grid independence study

One of the aims of the present numerical scheme is to show that the use of higher-order polynomials for approximating the partial differential equations requires relatively a coarse mesh to achieve benchmark solutions. This has great advantage while dealing with three-dimensional flow problems. In order to validate the computer program developed to solve the governing equations for the natural

Table 3
Numerical results for $Ra = 10^4$ at different angles

Ra		0°		15°		30°		45°		60°	
Nu_{mean}		2.2509		1.9858		1.6800		1.3913		1.1720	
Nu_{over}		2.0537		1.8425		1.5894		1.3434		1.1524	
10^4											
u_{max}	x		0.0000		0.0653		0.0653		0.1294		0.0653
	y	16.5312	0.5000	13.4033	0.5000	10.2433	0.5000	7.3206	0.3706	4.6810	0.3087
	z		0.1956		0.1956		0.1464		0.1464		0.1464
v_{max}	x		0.3967		0.3536		0.2500		0.0000		−0.1294
	y	2.1092	0.8044	1.4016	0.7500	0.7776	0.7500	0.4910	0.7500	0.3133	0.7500
	z		0.1464		0.1464		0.1033		0.1033		0.1033
w_{max}	x		0.3967		0.3967		0.3967		0.3967		0.3536
	y	18.6971	0.3087	15.6796	0.3087	12.0352	0.3087	8.3556	0.4347	5.1963	0.5000
	z		0.5000		0.4347		0.4347		0.4347		0.4347
u_{mmax}	x	1.4310	0.0000	13.4033	0.0653	10.2433	0.0653	7.3057	0.0653	4.6223	0.0653
	z		0.1956		0.1956		0.1464		0.1464		0.1464
w_{mmax}	x	1.4519	0.3044	15.5214	0.3967	11.9774	0.3967	8.3523	0.3967	5.1963	0.3536
	z		0.5000		0.4347		0.4347		0.4347		0.4347

Table 4
Numerical results for $Ra = 10^5$ at different angles

Ra		0°		15°		30°		45°		60°	
Nu_{mean}		4.6110		3.9690		3.0241		2.0385		1.3840	
Nu_{over}		4.3329		3.7731		2.9014		1.9791		1.3623	
10^5											
u_{max}	x		−0.1913		−0.1913		0.3044		0.3536		0.3044
	y	43.6877	0.2500	27.3932	0.3087	22.2297	0.1956	16.1999	0.1464	9.8207	0.1464
	z		0.1033		0.1464		0.1033		0.0670		0.0670
v_{max}	x		0.4330		0.3967		0.3536		0.3967		0.3967
	y	9.3720	0.8536	6.3100	0.8536	3.6066	0.8536	1.7519	0.1956	0.8845	0.1956
	z		0.1033		0.1033		0.0670		0.4347		0.3087
w_{max}	x		0.4330		0.4330		0.4330		0.4330		0.4330
	y	70.6267	0.1464	57.5766	0.1464	41.1468	0.1464	24.9537	0.1956	13.2210	0.2500
	z		0.5000		0.4347		0.3706		0.3087		0.3087
u_{mmax}	x	42.7846	−0.1913	26.8051	−0.1913	21.7375	0.3044	15.7396	0.3536	9.3477	0.3044
	z		0.1033		0.1464		0.1033		0.0670		0.0670
w_{mmax}	x	65.3083	0.4330	54.3757	0.4330	39.6992	0.4330	24.4660	0.4330	13.0699	0.4330
	z		0.5000		0.4347		0.3706		0.3087		0.3087

Table 5
Numerical results for $Ra = 10^6$ at different angles

Ra		0°		15°		30°		45°		60°	
Nu_{mean}		8.9098		7.5445		5.3303		2.8754		1.5829	
Nu_{over}		8.6678		7.3630		5.2133		2.8202		1.5585	
10^6											
u_{max}	x		−0.3044		0.3967		0.4330		0.4330		0.3967
	y	127.3724	0.1956	57.8944	0.1464	50.1269	0.1033	35.9581	0.0670	21.4072	0.0670
	z		0.0670		0.0670		0.0381		0.0381		0.0381
v_{max}	x		0.4619		0.4619		0.4330		0.3967		0.3536
	y	24.7203	0.8967	15.9619	0.9330	10.5337	0.9330	4.9564	0.9330	2.7513	0.8967
	z		0.1033		0.0670		0.0381		0.0381		0.0670
w_{max}	x		0.4619		0.4619		0.4619		0.4619		0.4619
	y	235.4754	0.0670	189.5337	0.0670	131.4209	0.1033	71.0999	0.1033	37.8190	0.1464
	z		0.4347		0.3706		0.3087		0.2500		0.2500
u_{mmax}	x	123.3556	−0.3044	55.4034	0.3967	48.6352	0.4330	35.1276	0.4330	20.7674	0.3967
	z		0.0670		0.0670		0.0381		0.0381		0.0381
w_{mmax}	x	217.6959	0.4619	179.0765	0.4619	126.3809	0.4619	68.7421	0.4619	36.7391	0.4619
	z		0.5000		0.3706		0.3087		0.2500		0.2500

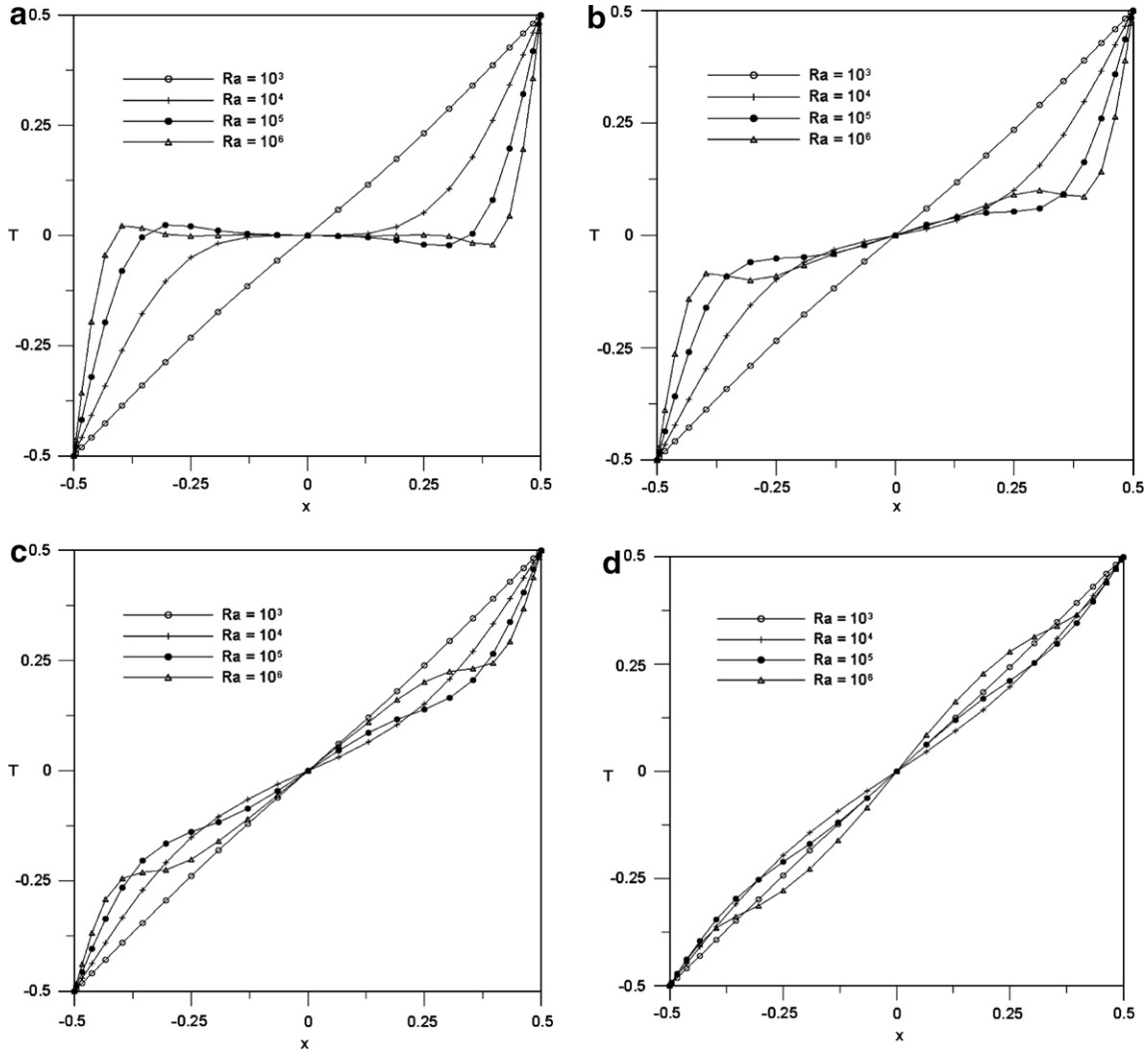

Fig. 2. Temperature profiles in the centerline of the symmetry plane at $y = 0.5$ for (a) $\phi = 0°$, (b) $\phi = 15°$, (c) $\phi = 30°$, (d) $\phi = 45°$.

convection problem, initially a grid independence study was carried out for $Ra = 10^3$, 10^4, 10^5, 10^6. The Nusselt number Nu is one of the important dimensionless parameters in heat transfer analysis of natural convection problems. The mean and the overall Nusselt number values are computed as

1. The mean Nusselt number throughout the cavity

$$Nu_{\text{mean}}(y) = \int_0^1 \frac{\partial T(y,z)}{\partial x}\bigg|_{x=-0.5,\text{ or } x=0.5} \mathrm{d}z. \tag{22}$$

2. The overall Nusselt number on the boundary at $x = -0.5$ or $x = 0.5$

$$Nu_{\text{overall}} = \int_0^1 Nu_{\text{mean}}(y)\mathrm{d}y. \tag{23}$$

Further, in order to make sure that the grid independence study is in accordance with other numerical results, the grid independence study results obtained for the case of $\phi = 0$ were compared with the results of Tric et al. [14] who used pseudo-spectral Chebyshev algorithm based on the projection-diffusion method with a spatial resolution supplied by polynomial expansions. For the mesh sensitivity study, the mean and the overall Nusselt number values were computed for $10^3 \leqslant Ra \leqslant 10^6$ using four different meshes of size 21^3, 23^3, 25^3 and 41^3. The value of Prandtl number was assumed as 0.71 for all these computations. Table 1 depicts the comparisons between the values of the mean and the overall Nusselt numbers obtained using the present method for the four mesh sizes and the results obtained by Tric et al. [14]. It can be observed that the results obtained by using the present numerical algorithm with the above four grids of size are almost in excellent agreement with the results of Tric et al. [14] for all the values of the Rayleigh numbers considered in this study. Even for the minimum grid size 21^3, no difference is observed between the values of the mean and the overall Nusselt numbers obtained by the four grid system. This clearly demonstrates that the DQ method used for the solution

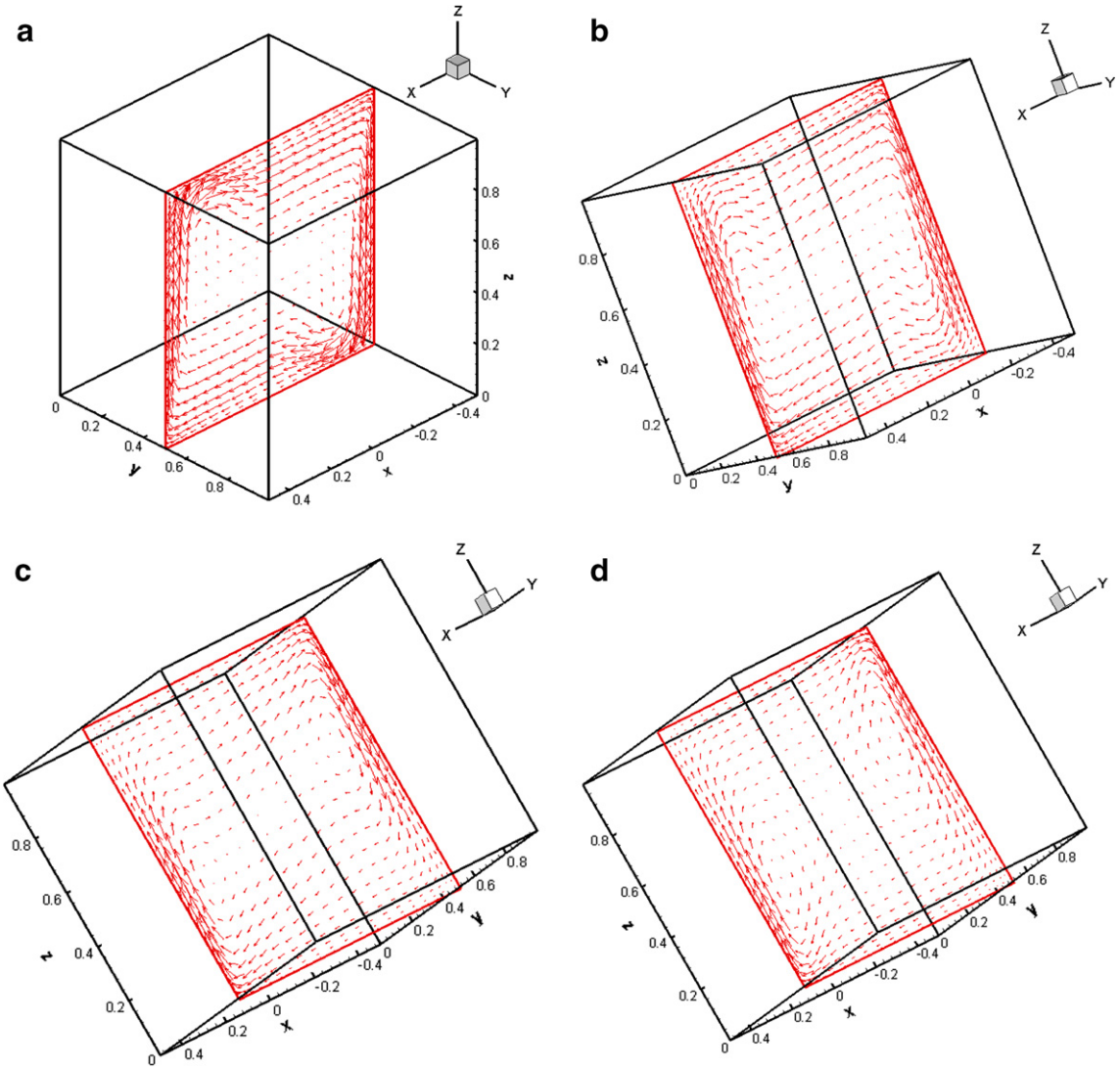

Fig. 3. Velocity vectors at $y = 0.5$ plane for $Ra = 10^6$ in a different angle (a) $\phi = 0°$, (b) $\phi = 15°$, (c) $\phi = 30°$, (d) $\phi = 45°$.

of the velocity–vorticity form of the Navier–Stokes equations can predict the Nusselt number values accurately even with a coarse mesh and the scheme is independent of spatial discretization with a minimum grid size of 21^3.

5.2. Effect of angle of inclination on natural convection phenomenon

Numerical results of the Nusselt numbers for different angle of inclination of the cavity are shown in Tables 2–5, for $Ra = 10^3$, 10^4, 10^5, 10^6, respectively. We also present results for the maximum values of velocities along with the maximum value of velocity for the symmetric mid-planes on the principal planes in the above tables. With increase in the angle of inclination, the buoyancy force decreases resulting in poor free convection phenomenon inside the cavity. This is clearly indicated by the decreasing trend of the Nusselt number values with increase in the angle of inclination as observed in the above tables for all the values of the Rayleigh numbers.

For the natural convection problem in a cavity with no-slip velocity boundary conditions on all the boundary walls, the only driving force is the buoyancy force, which is generated by the difference in density of the fluid and the vertical gravitational field in the z-direction. The variation in the density is due to the change in temperature at the left and the right walls, which were subjected to -0.5 and 0.5, respectively in the present case. The capability of the present numerical scheme can be tested by plotting the temperature variations along the x-coordinate as shown in Fig. 2 for different values of the Rayleigh number and angle of inclination, ϕ. As the angle of inclination increases, the buoyancy force is not sufficient enough to generate the convective current of the fluid. Hence the expected increased fluid convection due to increase in the Rayleigh number value is not observed in the above figures. The temperature gradient, which is linear for heat diffusion is clearly predicted by the present numerical algorithm as depicted in Fig. 2(d) at $\phi = 45°$. With increase in the Rayleigh number, initially the convective currents are

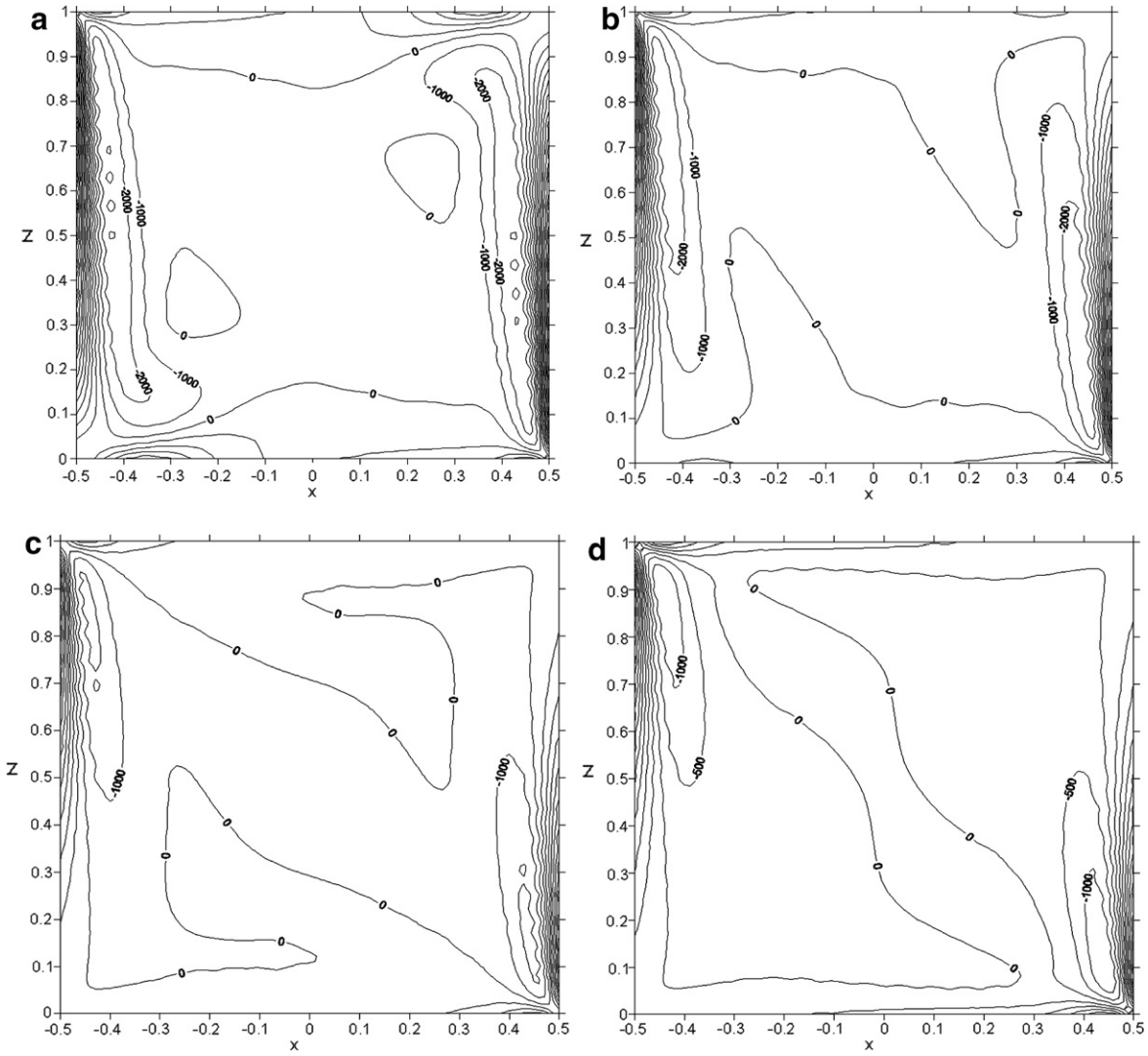

Fig. 4. Vorticity contours at $y = 0.5$ plane for $Ra = 10^6$ in a different angle (a) $\phi = 0°$, (b) $\phi = 15°$, (c) $\phi = 30°$, (d) $\phi = 45°$.

slowly set up in the flow field near the cold and the hot walls for all the four values of the Rayleigh number. The temperature gradient of the cavity almost reaches linear distributions at $10^3 \leqslant Ra \leqslant 10^6$ due to the increase in the angle of inclination.

Natural convection in a differentially heated cubic enclosure at different angle of inclination involves a vortex-dominated flow and this problem serves as a test case for any new CFD code. An important aspect of this problem is that the fluid movement takes place purely due to the buoyancy forces generated due to the temperature difference between the end walls. The present formulation based on the velocity–vorticity equations and the DQ method requires only the velocity and the temperature boundary conditions to be specified on the cavity walls because the vorticity values at the boundary are computed implicitly in the proposed coupled formulation. Apart from testing the code for the present formulation with respect to the Nusselt numbers, it is also required to verify for the flow fields, such as the velocity vectors, vorticity contour and temperature distributions as predicted by the present method. The characteristics of the natural convection phenomenon can be well understood by plotting the velocity vectors on the various symmetric mid-planes along the principal axes. Fig. 3(a)–(d) represents the velocity vectors plotted on x–z plane at $y = 0.5$ symmetric plane of the cavity for $\phi = 0°$, 15°, 30°, 45°, respectively at $Ra = 10^6$. As the angle of inclination increases the effect of decreased buoyancy forces is felt on the flow pattern. With increase in the angle of inclination, the velocity gradient decreases near the vertical walls as observed in the above figures.

The circulatory gyre pattern for natural convection in a cubic cavity can be more vividly captured using the vorticity contours on the mid-planes along the principal axes. Fig. 4(a)–(d) shows the vorticity contours plotted on the x–z plane at $y = 0.5$ for the angle of inclination varying from 0° to 45° at $Ra = 10^6$. As observed in the vorticity distribution, the vorticity generated at the boundaries are clearly shown in the above figures. With increase in the angle of inclination, the intensity of vorticity generation is observed to shift from the left and the right walls to top left corner and the bottom right corner. These changes indirectly indicate the variations in the velocity gradients due to the varying angle of inclination.

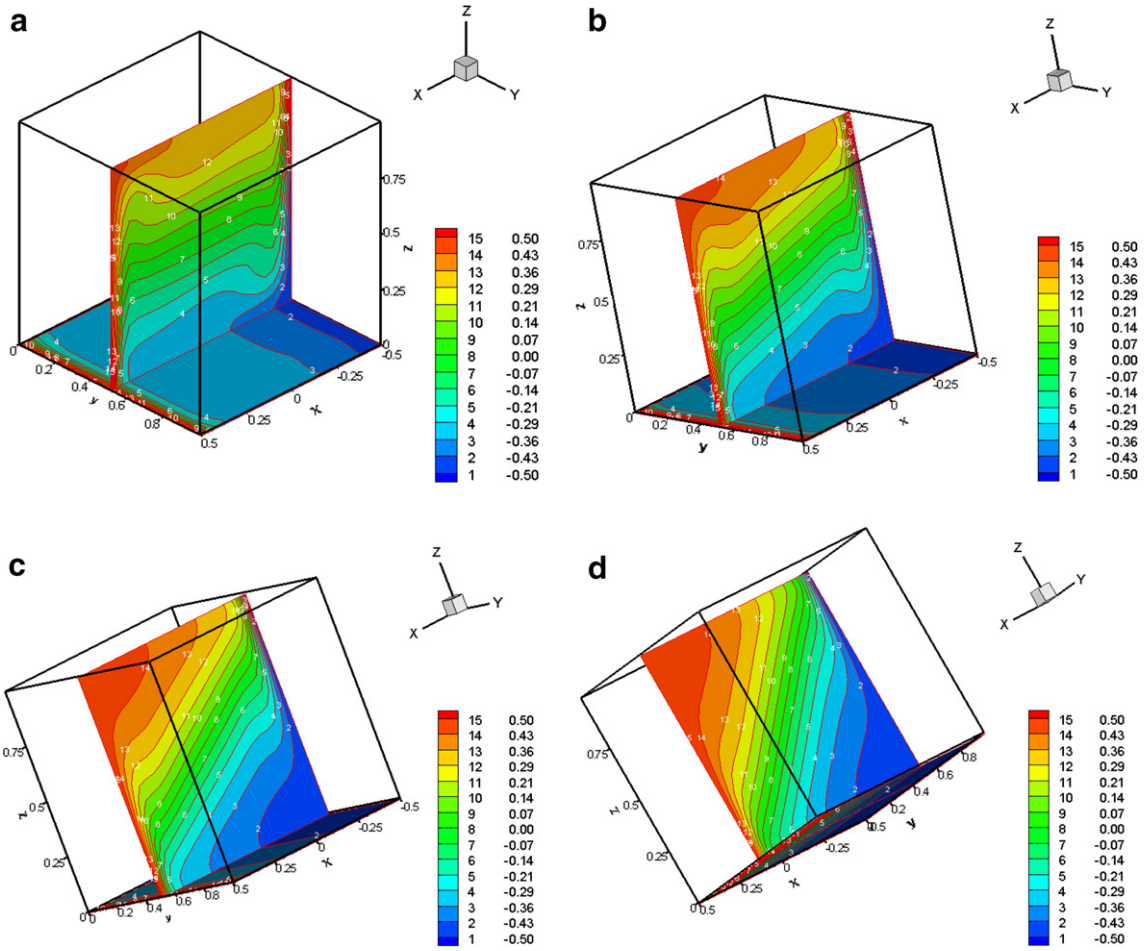

Fig. 5. Contour maps of temperature at $y = 0.5$ plane for $Ra = 10^6$ in a different angle (a) $\phi = 0°$, (b) $\phi = 15°$, (c) $\phi = 30°$, (d) $\phi = 45°$.

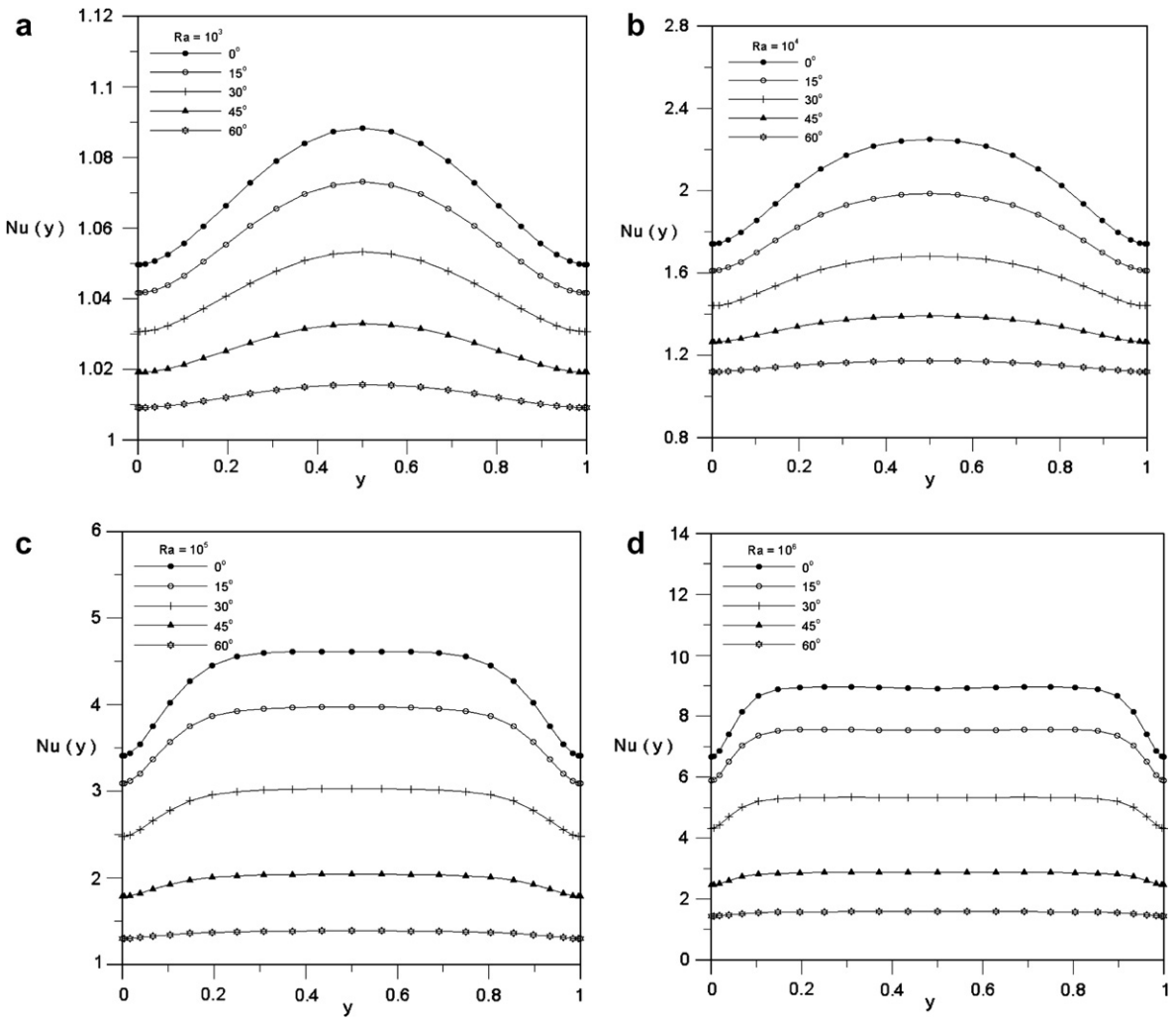

Fig. 6. Distribution of the mean Nusselt number along the y-direction for (a) $Ra = 10^3$, (b) $Ra = 10^4$, (c) $Ra = 10^5$, (d) $Ra = 10^6$.

In order to capture the three-dimensional effect of the temperature fields, the temperature variations on the mid-planes along the principal axes serve as a visual representation of the temperature variations throughout the cavity due to the buoyancy-induced flows. Fig. 5(a)–(d) shows the temperature contours on x–z plane at $y = 0.5$ for different angles of inclination for $Ra = 10^6$. As far as the convective heat transport is concerned this is the principal plane that indicates the heat transfer pheno-mena because this plane consists of the axes of the temp- erature differentials and the gravitational direction. The temperature maps are very close to the hot and the cold walls compared to the other sides, because greater temperature gradients are observed only at these regions. As the other sides are kept adiabatic, the temperature contours are always normal to these sides as observed in the above figures. Further the increase in the angle of inclination results in diagonally parallel isotherms instead of the nearly horizontal isotherms observed at $\phi = 0°$.

Nusselt number is an important non-dimensional parameter in convective heat transfer study. The mean value of the Nusselt number computed for the isothermal walls are shown as variations along the y-direction in Fig. 6(a)–(d) for $Ra = 10^3$, 10^4, 10^5, 10^6, respectively. An initial look on the range of the Nusselt number values shown on these figures clearly indicates that the Nusselt number increases with increase in the value of the Rayleigh number as expected. A symmetric variation is observed in all these figures. However the number of peaks and their positions vary with the value of the Rayleigh number. The maximum value of the Nusselt number is achieved only for $\phi = 0°$ as expected. As the angle of inclination increases, the maximum value of the Nusselt number decreases as seen from these figures. The tabular values of the Nusselt numbers shown in Tables 2–5 also support these trends. The results discussed for the inclined cavity demonstrate that the present numerical algorithm has correctly predicted the convective heat transport process inside the cavity for different values of angle of inclination. The proposed algorithm could enforce the vorticity boundary values implicitly. This fact is verified by the expected results predicted by the present algorithm for the flow and the temperature fields.

6. Conclusion

A coupled numerical algorithm based on the velocity–vorticity formulation and the DQ method was tested for natural convection in a differentially heated inclined cubic cavity. As regard to the velocity–vorticity equations and the boundary conditions this problem possesses some unique characteristics. Natural convection phenomenon couples the momentum equations with the energy equation through the buoyancy term using the Boussinesq approximation. In the case of velocity–vorticity formulation the velocity and the vorticity are already coupled together. Additionally, the natural convection process couples the temperature with the momentum equations, thus making the velocity, vorticity and temperature fields form a fully coupled system of equations. Since we propose a coupled numerical solution algorithm without explicit specification of the vorticity boundary values, the coupled natural convection problem could be treated as a suitable test case to validate the present numerical scheme. With regard to the boundary conditions, the boundary values for the velocity and temperature only need to be enforced for the natural convection problem, since the vorticity values are computed naturally from the known velocity fields in the coupled system. This makes the solution algorithm very unique compared to a scheme where the primitive variable form of the Navier–Stokes equations is used. Test results obtained for Rayleigh number in the range from 10^3 to 10^6 at the angle of incidence ($\phi = 0°$) show close agreements with other numerical scheme, producing the expected flow and temperature fields. Moreover, the salient characteristics of the different angle of incidence, $\phi = 15°$, 30°, 45°, 60° of natural convection in an inclined cavity are well-illustrated in the present study.

Acknowledgements

The support under Grant NSC 94-2218-E-464-001, 93-2611-E-002-017 and 94-2211-E-464-003 by the National Science Council of Taiwan is gratefully acknowledged.

References

[1] H. Fasel, Investigation of the stability of boundary layers by a finite-difference model of the Navier–Stokes equations, J. Fluid Mech. 78 (1976) 355–383.
[2] O. Daube, Resolution of the 2D Navier–Stokes equations in velocity–vorticity form by means of an influence matrix technique, J. Comput. Phys. 103 (1992) 402–414.
[3] G. Guj, F. Stella, A vorticity–velocity method for the numerical solution of 3D incompressible flows, J. Comput. Phys. 106 (1993) 286–298.
[4] D.C. Lo, D.L. Young, K. Murugesan, GDQ method for natural convection in a square cavity using a velocity–vorticity formulation, Numer. Heat Transfer, Part B 48 (2005) 363–386.
[5] D.C. Lo, K. Murugesan, D.L. Young, Numerical solution of three-dimensional velocity–vorticity Navier–Stokes equations by finite difference method, Int. J. Numer. Methods Fluids 47 (2005) 1469–1487.
[6] K.L. Wong, A.J. Baker, A 3D incompressible Navier–Stokes velocity–vorticity weak form finite element algorithm, Int. J. Numer. Methods Fluids 38 (2002) 99–123.
[7] X.H. Wu, J.Z. Wu, J.M. Wu, Effective vorticity–velocity formulations for three-dimensional incompressible viscous flows, J. Comput. Phys. 122 (1995) 68–82.
[8] R.E. Bellman, B.G. Kashef, J. Casti, Differential quadrature: a technique for the rapid solution of nonlinear partial differential equations, J. Comput. Phys. 10 (1972) 40–52.
[9] C. Shu, B.E. Richards, Application of generalized differential quadrature to solve 2-dimensional incompressible Navier–Stokes equations, Int. J. Numer. Methods Fluids 15 (1992) 791–798.
[10] C. Shu, H. Xue, Comparison of two approaches for implementing stream function boundary conditions in DQ simulation of natural convection in a square cavity, Int. J. Heat Fluid Flow 19 (1998) 59–68.
[11] K.M. Liew, T.M. Teo, Modeling via differential quadrature method: three-dimensional solutions for rectangular plates, Comput. Methods Appl. Mech. Eng. 159 (1998) 369–381.
[12] C. Shu, Differential Quadrature and its Application in Engineering, Springer, London, 2000.
[13] W.H. Press, S.A. Teukolsky, W.T. Vetterling, B.P. Flannery, Numerical Recipes in Fortran 90, 2nd ed., Cambridge University Press, New York, 1996.
[14] E. Tric, G. Labrosse, M. Betrouni, A first incursion into the 3D structure of natural convection of air in a differentially heated cubic cavity, from accurate numerical solutions, Int. J. Heat Mass Transfer 43 (2000) 4043–4056.